

Article

Modulation Characteristics of Period-One Oscillations in Quantum Cascade Lasers

Binbin Zhao ¹, Yibo Peng ¹, Xingguang Wang ¹ and Cheng Wang ^{1,2,*}

¹ School of Information Science and Technology, ShanghaiTech University, Shanghai 201210, China; zhaobb@shanghaitech.edu.cn (B.Z.); pengyb@shanghaitech.edu.cn (Y.P.); wangxg@shanghaitech.edu.cn (X.W.)

² Shanghai Engineering Research Center of Energy Efficient and Custom AI IC, ShanghaiTech University, Shanghai 201210, China

* Correspondence: wangcheng1@shanghaitech.edu.cn

Abstract: Quantum cascade lasers subject to tilted optical feedback produce periodic oscillations, quasi-periodic oscillations, and low-frequency oscillations. This work presents the modulation characteristics of period-one (P1) oscillations in a quantum cascade laser with tilted optical feedback. The electrical signal at the oscillation frequency is more than 50 dB higher than the noise level, and the electrical linewidth is less than 2.0 kHz. This electrical linewidth is about four orders of magnitude narrower than the optical linewidth (around 16 MHz) of the free-running laser, which suggests that the optical sidebands induced by the P1 oscillations are highly coherent with the main optical mode. In addition, the modulation depth of the optical signal is found to be in the range of 1% to 3.5%. In addition, it is verified in the simulations that the P1 oscillations induce not only amplitude modulation but also frequency modulation due to the phase-amplitude coupling effect.

Keywords: quantum cascade lasers; optical feedback; period-one oscillations; modulation characteristics



Citation: Zhao, B.; Peng, Y.; Wang, X.; Wang, C. Modulation Characteristics of Period-One Oscillations in Quantum Cascade Lasers. *Appl. Sci.* **2021**, *11*, 11730. <https://doi.org/10.3390/app112411730>

Academic Editor: Wilhelm Becker

Received: 25 October 2021

Accepted: 2 December 2021

Published: 10 December 2021

Publisher's Note: MDPI stays neutral with regard to jurisdictional claims in published maps and institutional affiliations.



Copyright: © 2021 by the authors. Licensee MDPI, Basel, Switzerland. This article is an open access article distributed under the terms and conditions of the Creative Commons Attribution (CC BY) license (<https://creativecommons.org/licenses/by/4.0/>).

1. Introduction

Semiconductor lasers subjected to external optical feedback usually produce rich nonlinear dynamics, including periodic oscillations, quasi-periodic oscillations, and chaotic oscillations [1]. Among these dynamics, chaos is the most well-known and has been used for applications of secure communication [2,3], random bit generation [4,5], Lidar systems [6], and reservoir computing networks [7,8]. One type of periodic oscillations, called period-one (P1) oscillations, have also been widely investigated. The P1 oscillations of common laser diodes originate from the undamped relaxation resonance oscillation and exhibit a sinusoidal-wave-like waveform [9–12]. Therefore, the P1 oscillations have been explored for the generation of high-frequency photonic microwaves. In comparison with common quantum well lasers, mid-infrared quantum cascade lasers (QCLs) are found to be highly stable against optical feedback due to their picosecond carrier lifetime [13–15]. Our previous work significantly narrowed the spectral linewidth of a QCL, based on its high stability, by using strong optical feedback [16]. However, QCLs with optical feedback did produce low-frequency fluctuations, or chaos, under peculiar operation conditions, such as near-threshold pump current, pulsed pump current, and low operation temperature [17–20]. Interestingly, a secure communication link using the chaos of a QCL has been demonstrated at a bit rate of 0.5 Mbit/s [21]. Our recent work found that QCLs can be more easily destabilized by using tilted optical feedback, where the reflection mirror is misaligned from the optical path [22]. In this configuration, we have observed periodic oscillations, quasi-periodic oscillation, and low-frequency oscillations at different mirror-tilt angles [22,23].

QCLs have been employed for gas sensing applications using a large variety of spectroscopy techniques [24]. Among these techniques, the modulation spectroscopy

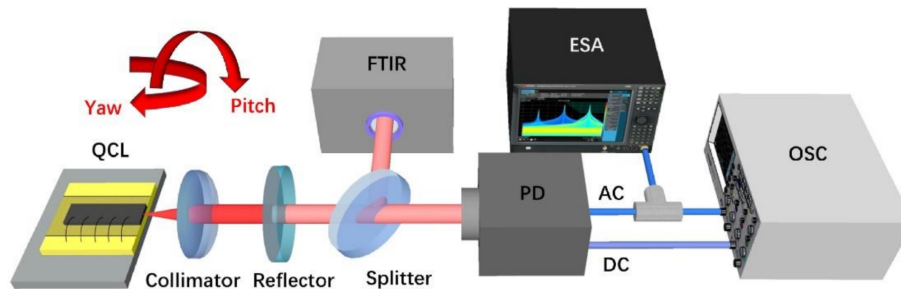
requires a sinusoidal modulation of the laser sources, including wavelength modulation spectroscopy (WMS) [25], frequency modulation spectroscopy (FMS) [26], and heterodyne phase-sensitive dispersion spectroscopy (HPSDS) [27,28]. The QCLs are usually modulated by direct current modulation or by external modulation using modulators [27,29–31] with modulation frequencies ranging from kHz up to several GHz [25–29,32]. Since the P1 oscillations also modulate the light in a sinusoidal waveform, this modulation might be helpful for developing modulation spectroscopy systems. Motivated by the above applications, this work investigates the modulation characteristics of P1 oscillations in a QCL with tilted optical feedback. It is found that the electrical signal induced by the P1 modulation is 50 to 65 dB higher than the noise level, and the modulation depth is in the range of 1% to 3.5%. The electrical linewidth is less than 2.0 kHz, although the optical linewidth of the free-running QCL is as high as 16 MHz. In addition, we also numerically demonstrate that the P1 oscillations also induce frequency modulation due to the phase-amplitude coupling effect.

2. Experimental Setup and Results

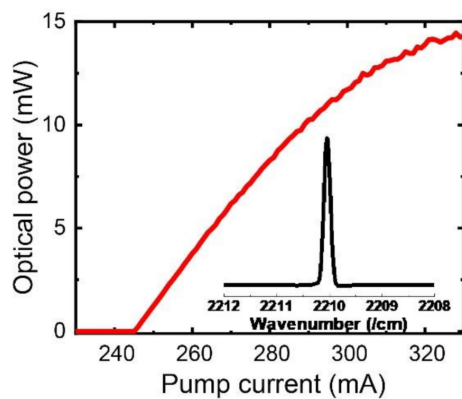
The QCL under study was grown on an InP substrate by solid-source molecular beam epitaxy [33]. The active region of the laser consists of 30 stages of InGaAs/InAlAs quantum wells. The laser has a ridge width of 8.5 μm and a cavity length of 2.0 mm. The first-order buried distributed feedback grating is fabricated on the upper InGaAs layer for achieving the single-mode emission. The front facet of the laser has an anti-reflection coating with a reflectivity of 1%, and the rear facet has a high-reflection coating with a reflectivity of 95%. Figure 1a shows the experimental setup for the generation of P1 oscillations. The QCL is powered by a low-noise current source (Newport, LDC-3736), and the operation temperature is maintained at 20 $^{\circ}\text{C}$ by using a thermo-electric cooler. The emitted light is collimated by an aspherical lens with a focal length of 4.0 mm. The optical feedback is provided by a reflector with a reflectivity of 47.5% that is placed about 61 cm away from the QCL. The tilt-angle of the reflector is finely adjusted in the yaw direction for the excitation of P1 oscillations. The optical spectrum is measured by a high-resolution (0.08/cm) Fourier transform infrared spectrometer (FTIR, Bruker Vertex 80). The optical signal is detected by an HgCdTe photodetector with a nominal bandwidth of 560 MHz. The temporal waveform is recorded on a digital oscilloscope (OSC, Keysight DSOS604A, 6 GHz bandwidth), and the electrical spectrum is measured on an electrical spectrum analyzer (ESA, Keysight N9040B, 50 GHz bandwidth). As shown in Figure 1b, the free-running QCL exhibits a lasing threshold of 245 mA and emits a single mode around 2210/cm or 4.53 μm (see inset). The optical linewidth is extracted from the analysis of the measured frequency noise spectrum [16]. Figure 1c shows that the optical linewidth is around 16 MHz. The slight increase in the linewidth with the pump current can be attributed to the non-uniform carrier distribution induced by the spatial hole-burning effect [34,35]. On the other hand, the small fluctuations of the linewidth at 270 mA and 290 MA are due to the fact that the operation temperature is slightly tuned at each pump current to meet the frequency requirement of the frequency discriminator [16,36].

When the reflector in Figure 1a is well aligned with the optical path (tilt angle is zero), the QCL remains stable and produces continuous-wave output. When the reflector is tilted in the yaw direction, however, the QCL loses its stability and produces periodic oscillations at small tilt angles, quasi-periodic oscillations at moderate angles, and low-frequency oscillations at large angles. For details of the oscillation dynamics, refer to [22,23]. The generation of the above nonlinear dynamic is attributed to the non-degeneracy of odd-order round-trip reflections with the even-order specimens, which arises from the tilted optical feedback [37,38]. This work focuses on the P1 dynamic, which is a type of periodic oscillation with only one period in the temporal waveform. Figure 2a shows that the P1 oscillation of the QCL exhibits a sinusoidal waveform, which is similar to the waveform of lasers with direct sinusoidal current modulation. The electrical spectrum in Figure 2b shows that the modulation frequency of the laser is 246.5 MHz. This modulation

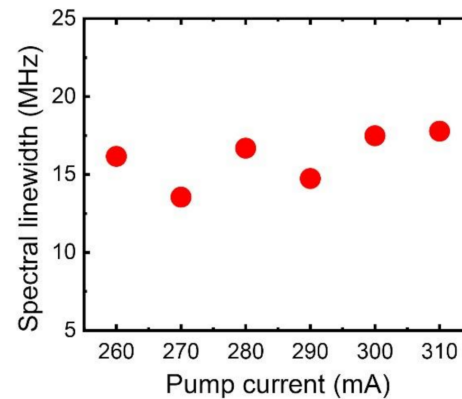
frequency equals the exact external cavity frequency, which is the inverse of the round-trip propagation time from the QCL to the reflector. Therefore, the P1 oscillation frequency is solely determined by the external cavity frequency due to the absence of relaxation oscillation resonance in QCLs [39]. This differs from common near-infrared laser diodes, where the P1 frequency is governed by the interaction of the relaxation oscillation frequency and the external cavity frequency [1].



(a)

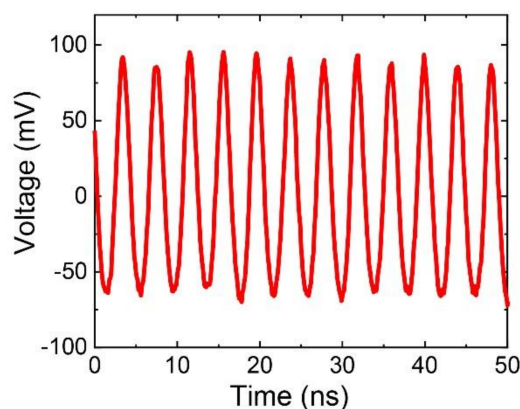


(b)

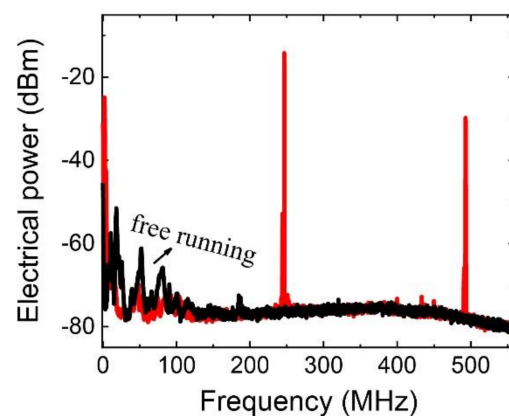


(c)

Figure 1. (a) Experimental setup for the modulation using P1 dynamics. FTIR, Fourier transform infrared spectrometer; PD, photodetector; ESA, electrical spectrum analyzer; OSC, oscilloscope. (b) L-I curve. Inset is the optical spectrum at 280 mA. (c) Optical linewidth versus the pump current. The reflector in (a) is tilted in the yaw direction. The tilt angle is zero when the reflector is well aligned with the optical path and is positive when the reflector is tilted in the arrow direction.



(a)



(b)

Figure 2. (a) Temporal waveform and (b) electrical spectrum of the P1 oscillation at 300 mA. The tilt angle of the reflector is -1.05° .

Figure 3a shows that the amplitudes of the fundamental signal in the electrical spectrum are mostly in the range of 50 to 65 dB, which yields an average value of 57.2 dB. The amplitude does not show clear dependence on either the tilt angle of the reflector or on the pump current of the laser. Through least-square fitting of the electrical signal using the Voigt function, we obtain the electrical linewidth as illustrated in the inset of Figure 3b. For the statistics of the linewidth, 20 sweeps of measurement are averaged for every tilt angle with a resolution bandwidth (RBW) of 2.0 kHz. It is demonstrated that the electrical linewidths for different tilt angles in Figure 3b are mostly in the range of 1.5 to 2.0 kHz, with an average value of 1.7 kHz. It is remarked that these extracted linewidths are below the RBW of 2.0 kHz. However, a smaller RBW leads to an electrical signal deviating from the Voigt shape. In this case, the fundamental signal peak splits into several sub-peaks due to the long-term instability of the experimental setup, such as the variation of the feedback length or phase [40]. This P1 frequency instability will be quantified in future work. On the other hand, the frequency stability can be improved by stabilizing the feedback mirror position using a piezoelectric transducer. Similar to the peak amplitude in Figure 3a, the electrical linewidth is almost independent of the tilt angle and of the pump current as well. Surprisingly, the electrical linewidth of the P1 oscillations is about four orders of magnitude smaller than the optical linewidth of the free-running laser. Because the electrical spectrum is a beat note of the optical spectrum, the ultra-narrow electrical linewidth suggests that the main optical mode is highly coherent with the P1-induced optical sidebands. Unluckily, these sidebands are not visible in the optical spectrum due to the resolution limit of the FTIR (2.4 GHz). Future work may measure such optical sidebands based on the absorption resonance of certain gas molecules [41,42]. The high coherence of the optical sidebands is similar to that with direct current modulation or with external modulation. It is remarked that semiconductor lasers subject to optical injection produce P1 oscillations as well [43,44]. However, the coherence of the optical sidebands with optical injection is usually low and varies significantly depending on the injection condition [9,11]. Figure 4 extracts the modulation depth of the electrical signal from the AC temporal waveform in Figure 2a, along with the tracked DC voltage. The modulation depths are mostly in the range of 1.0% to 3.5%. The dependence of the modulation depth on the tilt angle of the reflector is not obvious, possibly due to the uncertainty of the measured tilt angle, including the calibration error of zero angle and the backlash of the kinematic stage. On the other hand, the modulation depth shows little dependence on the pump current.

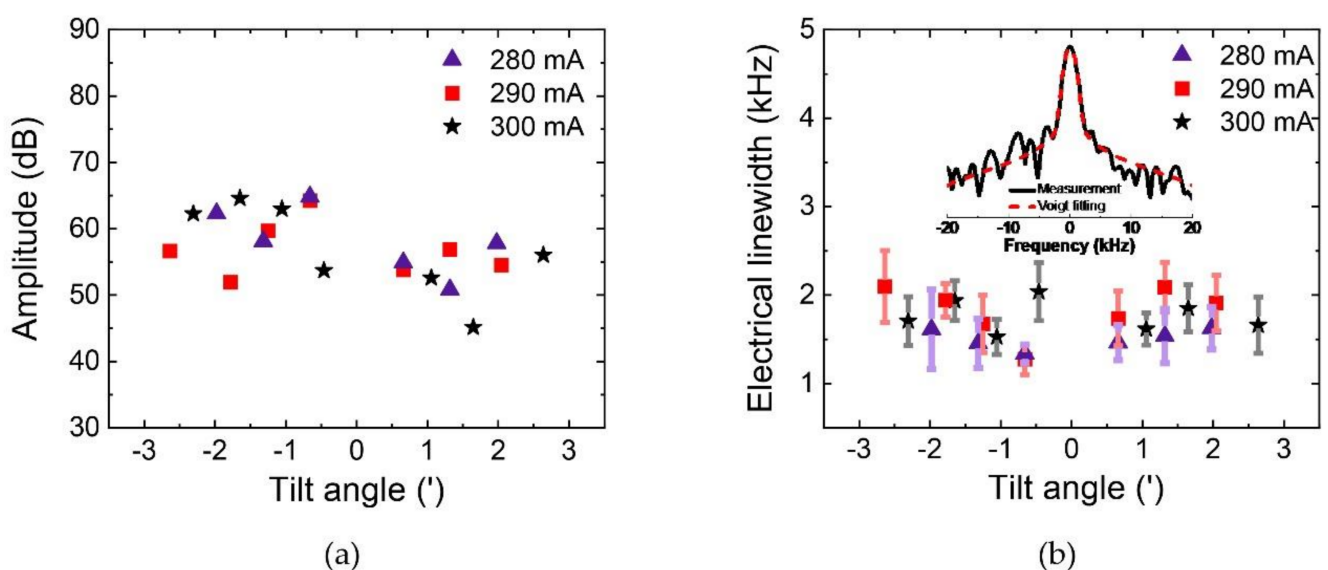


Figure 3. (a) Amplitude and (b) linewidth of the fundamental electrical signal for pump currents of 280, 290, and 300 mA. Inset is an example of the electrical linewidth fitting using the Voigt function.

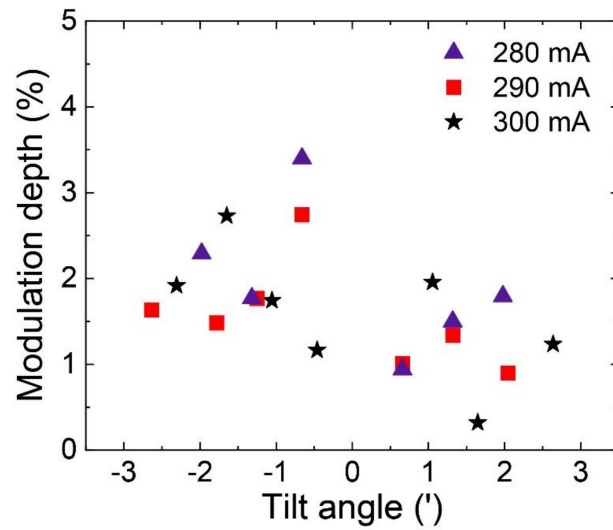


Figure 4. Modulation depth of the temporal waveform for pump currents of 280, 290, and 300 mA.

Because the P1 frequency is governed by the external cavity frequency, the modulation frequency of the QCL can be easily tuned by changing the feedback length. As shown in Figure 5, the P1 frequency is tuned from 147.1 MHz at the feedback length of about 102 cm up to 627.3 MHz at the length of about 24 cm, which is the lower length limit of our experimental setup. Further optimizing the setup in future work can achieve the modulation frequency up to the GHz range.

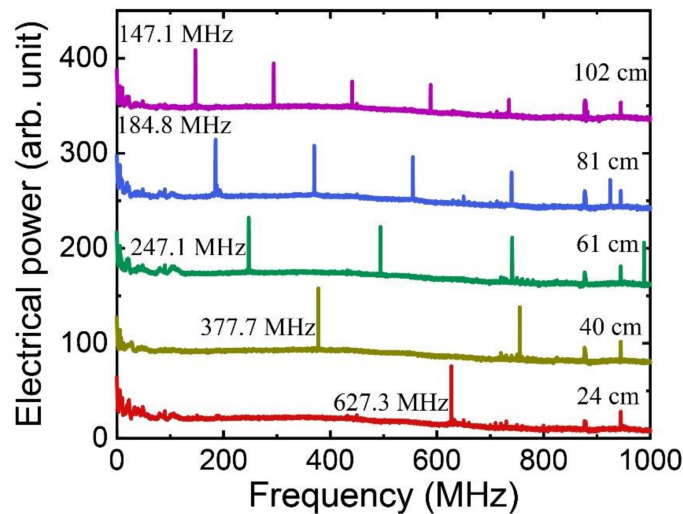


Figure 5. Electrical spectra of P1 oscillations for various single-trip feedback lengths. The pump current is 290 mA.

3. Simulations and Discussion

In order to show the optical sidebands induced by the P1 oscillation, we simulate the optical spectrum using the rate equation approach, which takes into account the effect of tilted optical feedback [22,23,37]. Rate equations for the photon number $S(t)$ and the phase of the electric field $\phi(t)$ are given by

$$\frac{dS}{dt} = \left(mG_0\Delta N - \frac{1}{\tau_p} \right) S + m\beta \frac{N_3}{\tau_{sp}} + 2k_c f_n \sqrt{r_{ext} S(t)} \sum_{n=1}^{\infty} \left(\sqrt{R r_{ext}} \right)^{n-1} \sqrt{S(t - n\tau_{ext})} \cos(\Delta\phi_n) \quad (1)$$

$$\frac{d\phi}{dt} = \frac{\alpha_H}{2} \left(mG_0\Delta N - \frac{1}{\tau_p} \right) - \frac{2k_c f_n}{\sqrt{r_{ext} S(t)}} \sum_{n=1}^{\infty} \left(\sqrt{R r_{ext}} \right)^{n-1} \sqrt{S(t - n\tau_{ext})} \sin(\Delta\phi_n) \quad (2)$$

with

$$f_n = \begin{cases} \frac{\sin(\theta\pi)}{\theta\pi} & \text{for } n = 1, 3, 5 \dots \\ 1 & \text{for } n = 2, 4, 6 \dots \end{cases} \quad (3)$$

where m is the number of cascading gain stages, G_0 is the gain coefficient, ΔN is the population inversion, τ_p is the photon lifetime, τ_{sp} is the spontaneous emission lifetime, β is the spontaneous emission factor, N_3 is the carrier number in the upper lasing level, α_H is the linewidth broadening factor (LBF), and R is the facet reflectivity. The feedback ratio is r_{ext} , τ_{ext} is the feedback delay time, and k_c is the feedback coupling coefficient to the laser cavity. The phase difference is $\Delta\phi_n = n\phi_0 + \phi(t) - \phi(t - n\tau_{ext})$, with ϕ_0 being the initial feedback phase, and n being the order of roundtrip reflection. The tilted angle of the reflection mirror is θ , which is normalized by the tilt angle at which the first diffractive coupling minimum occurs. Details of the rate equation model and the parameter values will be described elsewhere. Figure 6a simulates the optical spectrum of the QCL with P1 oscillation, where the LBF is 2.0 and the single-trip feedback length is 60 cm. It is shown that the laser exhibits multiple sidebands with a spacing of 250 MHz, which is determined by the P1 frequency or the external cavity frequency. The optical sidebands are asymmetric with respect to the main lasing mode due to the non-zero LBF. Because of this phase-amplitude coupling effect, the P1 oscillations introduce not only amplitude modulation (AM) but also frequency modulation (FM) [45]. Taking advantage of this feature, the P1 oscillations of near-infrared laser diodes have been used for the AM-to-FM conversion of photonic microwaves [46,47]. The LBF of the QCL under study increases almost linearly with the pump current, from 1.4 at 250 mA to 2.5 at 310 mA (see [23] for details). In comparison with the AM measurement in Figure 2, experimental characterization of the FM is much more challenging, usually requiring a frequency discriminator to convert the FM into AM [48]. Therefore, we confirm the existence of FM using rate Equations (1) and (2) as well. Based on the temporal waveform in Figure 6b, the FM index is deduced to be 17%, and the AM index (or the modulation depth) is 1.9%. Therefore, the P1 oscillation-induced modulation is dominated by the FM. This behavior is also similar to that of QCLs with direct current modulation, where the ratio of the AM index to the FM index is around 0.07 [49].

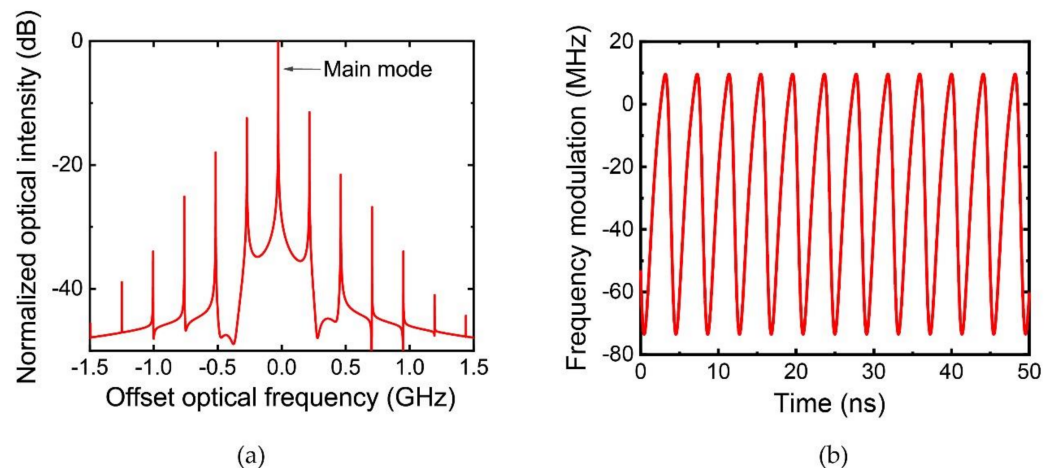


Figure 6. (a) Simulated optical spectrum and (b) frequency modulation of the QCL with P1 oscillation. The single-trip feedback length is 60 cm, and the LBF is 2.0.

Finally, we summarize the potential application of P1 oscillations in the modulation spectroscopy technique. The WMS usually requires a modulation frequency in the range of kHz to MHz [25,32], as well as a very large modulation depth [50–52]. However, the modulation characteristics of P1 oscillations described in this work deviate significantly from both required features; hence, it is difficult to apply P1 oscillations in WMS. On the other hand, the modulation frequency of HPSDS is in the range of MHz to GHz [25,32], and that of FMS is of 100 MHz to several GHz [26–29,32], respectively. Both modulation

frequencies can be easily reached by the P1 oscillations in QCLs. HPSDS mainly requires AM, while FMS requires FM, but the co-existence of AM and FM is allowed in both practical applications [27,50]. HPSDS requires only a small modulation depth, which satisfies the modulation characteristics of P1 oscillations [27,28]. In contrast, FMS requires a modulation depth spreading from several percent up to tens of percent for achieving optimal performance [50,53]. In this case, better methods should be pursued for tuning the modulation depth of P1 oscillations in future work.

4. Conclusions

In conclusion, we have unveiled the modulation characteristics of P1 oscillations in a QCL subject to optical feedback. The optical linewidth of the free-running QCL is about 16 MHz, while the electrical linewidth of the P1 oscillation is less than 2.0 kHz owing to the high coherence of the optical sidebands with the main optical mode. The modulation depths of the light are in the range of 1% to 3.5%, and the electrical signals at the modulation frequency are more than 50 dB higher than the background noise level. The P1 modulation frequency can be easily adjusted by tuning the feedback length. It is further confirmed in the simulation that P1 oscillation also induces FM in addition to AM due to the phase-amplitude coupling effect. Future work will study the detailed FM characteristics of the P1 oscillations in the experiment. We believe this work can pave the way for potential applications of P1 oscillations in the mid-infrared regime, such as gas sensing based on the modulation spectroscopy technique.

Author Contributions: C.W. initiated and supervised this study; B.Z. and Y.P. delivered the experiment; X.W. run the simulations. All authors have read and agreed to the published version of the manuscript.

Funding: This research was funded by National Natural Science Foundation of China (NSFC), grant number 61804095, and Shanghai Natural Science Foundation, grant number 20ZR1436500.

Institutional Review Board Statement: Not applicable.

Informed Consent Statement: Not applicable.

Data Availability Statement: The data presented in this study are available on request from the corresponding author.

Conflicts of Interest: The authors declare no conflict of interest.

References

1. Ohtsubo, J. *Semiconductor Lasers: Stability, Instability and Chaos*, 4th ed.; Springer: Berlin/Heidelberg, Germany, 2017.
2. Argyris, A.; Syvridis, D.; Larger, L.; Annovazzi-Lodi, V.; Colet, P.; Fischer, I.; García-Ojalvo, J.; Mirasso, C.R.; Pesquera, L.; Shore, K.A. Chaos-based communications at high bit rates using commercial fibre-optic links. *Nature* **2005**, *438*, 343–346. [[CrossRef](#)] [[PubMed](#)]
3. Van Wiggeren, G.D.; Roy, R. Communication with chaotic lasers. *Science* **1998**, *279*, 1198–1200. [[CrossRef](#)] [[PubMed](#)]
4. Uchida, A.; Amano, K.; Inoue, M.; Hirano, K.; Naito, S.; Someya, H.; Oowada, I.; Kurashige, T.; Shiki, M.; Yoshimori, S.; et al. Fast physical random bit generation with chaotic semiconductor lasers. *Nat. Photonics* **2008**, *2*, 728–732. [[CrossRef](#)]
5. Kanter, I.; Aviad, Y.; Reidler, I.; Cohen, E.; Rosenbluh, M. An optical ultrafast random bit generator. *Nat. Photonics* **2010**, *4*, 58–61. [[CrossRef](#)]
6. Lin, F.Y.; Liu, J.M. Chaotic radar using nonlinear laser dynamics. *IEEE J. Quantum Electron.* **2004**, *40*, 815–820. [[CrossRef](#)]
7. Van der Sande, G.; Brunner, D.; Soriano, M.C. Advances in photonic reservoir computing. *Nanophotonics* **2017**, *6*, 561–576. [[CrossRef](#)]
8. Nakayama, J.; Kanno, K.; Uchida, A. Laser dynamical reservoir computing with consistency: An approach of a chaos mask signal. *Opt. Express* **2016**, *24*, 8679–8692. [[CrossRef](#)]
9. Simpson, T.B.; Liu, J.M.; AlMulla, M.; Usechak, N.G.; Kovanis, V. Limit-cycle dynamics with reduced sensitivity to perturbations. *Phys. Rev. Lett.* **2014**, *112*, 023901. [[CrossRef](#)]
10. Wang, C.; Raghunathan, R.; Schires, K.; Chan, S.C.; Lester, L.F.; Grillot, F. Optically injected InAs/GaAs quantum dot laser for tunable photonic microwave generation. *Opt. Lett.* **2016**, *41*, 1153–1156. [[CrossRef](#)]
11. Lin, L.C.; Liu, S.H.; Lin, F.Y. Stability of period-one (P1) oscillations generated by semiconductor lasers subject to optical injection or optical feedback. *Opt. Express* **2017**, *25*, 25523–25532. [[CrossRef](#)]

12. Tseng, C.H.; Lin, C.T.; Hwang, S.K. V-and W-band microwave generation and modulation using semiconductor lasers at period-one nonlinear dynamics. *Opt. Lett.* **2020**, *45*, 6819–6822. [[CrossRef](#)]
13. Mezzapesa, F.P.; Columbo, L.L.; Brambilla, M.; Dabbicco, M.; Borri, S.; Vitiello, M.S.; Beere, H.E.; Ritchie, D.A.; Scamarcio, G. Intrinsic stability of quantum cascade lasers against optical feedback. *Opt. Express* **2013**, *21*, 13748–13757. [[CrossRef](#)]
14. Friart, G.; Van der Sande, G.; Verschaffelt, G.; Erneux, T. Analytical stability boundaries for quantum cascade lasers subject to optical feedback. *Phys. Rev. E Stat. Phys. Plasmas Fluids Relat. Interdiscip. Top.* **2016**, *93*, 052201. [[CrossRef](#)]
15. Zhao, B.B.; Wang, X.G.; Zhang, J.C.; Wang, C. Relative intensity noise of a mid-infrared quantum cascade laser: Insensitivity to optical feedback. *Opt. Express* **2019**, *27*, 26639–26647. [[CrossRef](#)]
16. Zhao, B.B.; Wang, X.G.; Wang, C. Strong optical feedback stabilized quantum cascade laser. *ACS Photon.* **2020**, *7*, 1255–1261. [[CrossRef](#)]
17. Jumpertz, L.; Schires, K.; Carras, M.; Sciamanna, M.; Grillot, F. Chaotic light at mid-infrared wavelength. *Light Sci. Appl.* **2016**, *5*, e16088. [[CrossRef](#)]
18. Spitz, O.; Wu, J.; Herdt, A.; Carras, M.; Elsässer, W.; Wong, C.W.; Grillot, F. Investigation of chaotic and spiking dynamics in mid-infrared quantum cascade lasers operating continuous-waves and under current modulation. *IEEE J. Sel. Top. Quantum Electron.* **2019**, *25*, 1200311. [[CrossRef](#)]
19. Qi, X.; Bertling, K.; Taimre, T.; Agnew, G.; Lim, Y.L.; Gillespie, T.; Robinson, A.; Brünig, M.; Demić, A.; Dean, P.; et al. Observation of optical feedback dynamics in single-mode terahertz quantum cascade lasers: Transient instabilities. *Phys. Rev. A* **2021**, *103*, 033504. [[CrossRef](#)]
20. Spitz, O.; Wu, J.; Carras, M.; Wong, C.; Grillot, F. Low frequency fluctuations of a mid-infrared quantum cascade laser operating at cryogenic temperatures. *Laser Phys. Lett.* **2018**, *15*, 116201. [[CrossRef](#)]
21. Spitz, O.; Herdt, A.; Wu, J.; Maisons, G.; Carras, M.; Wong, C.W.; Elsässer, W.; Grillot, F. Private communication with quantum cascade laser photonic chaos. *Nat. Commun.* **2021**, *12*, 3327. [[CrossRef](#)]
22. Wang, X.G.; Zhao, B.B.; Deng, Y.; Kovanis, V.; Wang, C. Nonlinear dynamics of a quantum cascade laser with tilted optical feedback. *Phys. Rev. A* **2021**, *103*, 023528. [[CrossRef](#)]
23. Zhao, B.B.; Wang, X.G.; Wang, C. Low-frequency oscillations in quantum cascade lasers with tilted optical feedback. *IEEE J. Sel. Top. Quantum Electron.* **2022**, *28*, 1800207. [[CrossRef](#)]
24. Faist, J.; Capasso, F.; Sivco, D.L.; Sirtori, C.; Hutchinson, A.L.; Cho, A.Y. Quantum cascade laser. *Science* **1994**, *264*, 553–556. [[CrossRef](#)] [[PubMed](#)]
25. Hancock, G.; Van Helden, J.H.; Peverall, R.; Ritchie, G.A.D.; Walker, R.J. Direct and wavelength modulation spectroscopy using a cw external cavity quantum cascade laser. *Appl. Phys. Lett.* **2009**, *94*, 201110. [[CrossRef](#)]
26. Silver, J.A. Frequency-modulation spectroscopy for trace species detection: Theory and comparison among experimental methods. *Appl. Opt.* **1992**, *31*, 707–717. [[CrossRef](#)] [[PubMed](#)]
27. Martín-Mateos, P.; Hayden, J.; Acedo, P.; Lendl, B. Heterodyne phase-sensitive dispersion spectroscopy in the mid-infrared with a quantum cascade laser. *Anal. Chem.* **2017**, *89*, 5916–5922. [[CrossRef](#)] [[PubMed](#)]
28. Wang, Z.; Cheong, K.P.; Li, M.; Wang, Q.; Ren, W. Theoretical and experimental study of heterodyne phase-sensitive dispersion spectroscopy with an injection-current-modulated quantum cascade laser. *Sensors* **2020**, *20*, 6176. [[CrossRef](#)] [[PubMed](#)]
29. Martín-Mateos, P.; Acedo, P. Heterodyne phase-sensitive detection for calibration-free molecular dispersion spectroscopy. *Opt. Express* **2014**, *22*, 15143–15153. [[CrossRef](#)]
30. Zhu, X.; Cassidy, D.T. Modulation spectroscopy with a semiconductor diode laser by injection-current modulation. *J. Opt. Soc. Am. B* **1997**, *14*, 1945–1950. [[CrossRef](#)]
31. Bjorklund, G.C. Frequency-modulation spectroscopy: A new method for measuring weak absorptions and dispersions. *Opt. Lett.* **1980**, *5*, 15–17. [[CrossRef](#)]
32. Bomse, D.S.; Stanton, A.C.; Silver, J.A. Frequency modulation and wavelength modulation spectroscopies: Comparison of experimental methods using a lead-salt diode laser. *Appl. Opt.* **1992**, *31*, 718–731. [[CrossRef](#)]
33. Zhang, J.C.; Liu, F.Q.; Tan, S.; Yao, D.Y.; Wang, L.J.; Li, L.; Liu, J.Q.; Wang, Z.G. High-performance uncooled distributed-feedback quantum cascade laser without lateral regrowth. *Appl. Phys. Lett.* **2012**, *100*, 112105. [[CrossRef](#)]
34. Wu, M.C.; Lo, Y.H.; Wang, S. Linewidth broadening due to longitudinal spatial hole burning in a long distributed feedback laser. *Appl. Phys. Lett.* **1988**, *52*, 1119–1121. [[CrossRef](#)]
35. Wenzel, H.; Wunsche, H.J.; Bandelow, U. Linewidth rebroadening in semiconductor lasers due to lateral spatial holeburning. *Electron. Lett.* **1991**, *27*, 2301–2302. [[CrossRef](#)]
36. Deng, Y.; Zhao, B.B.; Wang, X.G.; Wang, C. Narrow linewidth characteristics of interband cascade lasers. *Appl. Phys. Lett.* **2020**, *116*, 201101. [[CrossRef](#)]
37. Seo, D.S.; Park, J.D.; McInerney, J.G.; Osinski, M. Multiple feedback effects in asymmetric external cavity semiconductor lasers. *IEEE J. Quantum Electron.* **1989**, *25*, 2229–2238. [[CrossRef](#)]
38. Park, J.D.; Seo, D.S.; McInerney, J.G. Self-pulsations in strongly coupled asymmetric external cavity semiconductor lasers. *IEEE J. Quantum Electron.* **1990**, *26*, 1353–1362. [[CrossRef](#)]
39. Paiella, R.; Martini, R.; Capasso, F.; Gmachl, C.; Hwang, H.Y.; Sivco, D.L.; Baillargeon, J.N.; Cho, A.Y.; Whittaker, E.A.; Liu, H.C. High-frequency modulation without the relaxation oscillation resonance in quantum cascade lasers. *Appl. Phys. Lett.* **2001**, *79*, 2526–2528. [[CrossRef](#)]

40. Simpson, T.B.; Liu, J.M.; AlMulla, M.; Usechak, N.G.; Kovanis, V. Linewidth sharpening via polarization-rotated feedback in optically injected semiconductor laser oscillators. *IEEE J. Sel. Top. Quantum Electron.* **2013**, *19*, 1500807. [[CrossRef](#)]
41. Chen, W.L.; Chen, T.L.; Liu, Y.W. Sideband amplitude modulation absorption spectroscopy of CH₄ at 1170 nm. *Opt. Express* **2019**, *27*, 21264–21272. [[CrossRef](#)]
42. Zou, M.; Sun, L.; Li, S. Simultaneous measurement of gas absorption and path length based on the dual-sideband heterodyne phase-sensitive detection of dispersion spectroscopy. *Opt. Express* **2021**, *29*, 11683–11692. [[CrossRef](#)]
43. Hwang, S.K.; Liu, J.M.; White, J.K. Characteristics of period-one oscillations in semiconductor lasers subject to optical injection. *IEEE J. Sel. Top. Quantum Electron.* **2004**, *10*, 974–981. [[CrossRef](#)]
44. Chan, S.C.; Hwang, S.K.; Liu, J.M. Period-one oscillation for photonic microwave transmission using an optically injected semiconductor laser. *Opt. Express* **2007**, *15*, 14921–14935. [[CrossRef](#)]
45. Henry, C. Theory of the linewidth of semiconductor lasers. *IEEE J. Quantum Electron.* **1982**, *18*, 259–264. [[CrossRef](#)]
46. Chan, S.C.; Hwang, S.K.; Liu, J.M. Radio-over-fiber AM-to-FM upconversion using an optically injected semiconductor laser. *Opt. Lett.* **2006**, *31*, 2254–2256. [[CrossRef](#)]
47. Chu, C.H.; Lin, S.L.; Chan, S.C.; Hwang, S.K. All-optical modulation format conversion using nonlinear dynamics of semiconductor lasers. *IEEE J. Quantum Electron.* **2012**, *48*, 1389–1396. [[CrossRef](#)]
48. Hangauer, A.; Spinner, G.; Nikodem, M.; Wysocki, G. High frequency modulation capabilities and quasi single-sideband emission from a quantum cascade laser. *Opt. Express* **2014**, *22*, 23439–23455. [[CrossRef](#)]
49. Eichholz, R.; Richter, H.; Wienold, M.; Schrottke, L.; Hey, R.; Grahn, H.T.; Hübers, H.W. Frequency modulation spectroscopy with a THz quantum-cascade laser. *Opt. Express* **2013**, *21*, 32199–32206. [[CrossRef](#)]
50. Supplee, J.M.; Whittaker, E.A.; Lenth, W. Theoretical description of frequency modulation and wavelength modulation spectroscopy. *Appl. Opt.* **1994**, *33*, 6294–6302. [[CrossRef](#)]
51. Rieker, G.B.; Jeffries, J.B.; Hanson, R.K. Calibration-free wavelength-modulation spectroscopy for measurements of gas temperature and concentration in harsh environments. *Appl. Opt.* **2009**, *48*, 5546–5560. [[CrossRef](#)]
52. Sun, K.; Chao, X.; Sur, R.; Goldenstein, C.S.; Jeffries, J.B.; Hanson, R.K. Analysis of calibration-free wavelength-scanned wavelength modulation spectroscopy for practical gas sensing using tunable diode lasers. *Meas. Sci. Technol.* **2013**, *24*, 125203. [[CrossRef](#)]
53. Borri, S.; Bartalini, S.; De Natale, P.; Inguscio, M.; Gmachl, C.; Capasso, F.; Sivco, D.L.; Cho, A.Y. Frequency modulation spectroscopy by means of quantum-cascade lasers. *Appl. Phys. B* **2006**, *85*, 223–229. [[CrossRef](#)]